# Reconfigurable Floquet Elastodynamic Topological Insulators Based on Synthetic Angular Momentum Bias

Amir Darabi and Michael J. Leamy\*
Woodruff School of Mechanical Engineering, Georgia Institute of Technology, Atlanta, GA

Xiang Ni

Photonics Initiative, Advanced Science Research Center, City University of New York, New York, NY

Andrea Alù<sup>†</sup>

Photonics Initiative, Advanced Science Research Center, City University of New York, New York, NY and Physics Program, Graduate Center, City University of New York, New York, NY

Originating with the discovery of the quantum Hall effect (QHE) in condensed-matter physics 1-3, topological order has been receiving increased attention also for classical wave phenomena. Topological protection enables efficient and robust signal transport; mechanical topological insulators (TIs), in particular, are easy to fabricate and exhibit interfacial wave transport with minimal dissipation, even in the presence of sharp edges, defects or disorder<sup>4-6</sup>. Here, we report the first experimental demonstration of a phononic crystal Floquet topological insulator (FTI). Hexagonal arrays of circular piezoelectric disks bonded to a PLA substrate, shunted through negative electrical capacitance and manipulated by external integrated circuits, provide the required spatio-temporal modulation scheme to break time-reversal symmetry and impart a synthetic angular momentum bias that can induce topological order and strong topological protection on the lattice edges. By changing the modulation scheme, we also show topological domain reconfiguration, with exciting opportunities for robust multiplexing of elastic wave transport. Our proposed reconfigurable FTI may find applications for robust acoustic emitters, delay lines, and mechanical logic circuits, with distinct advantages over electronic equivalents in harsh operating conditions and/or low-power applications.

Topologically-ordered states, such as those induced by two-dimensional quantum Hall and quantum spin Hall effects, and three-dimensional topological insulators, have received significant attention in the past few years. Topological states of matter were first described in electronic materials using Fermi-Dirac statistics<sup>3,7-10</sup>, then in bosonic systems such as photonic crystals and classical waves in electromagnetic materials<sup>11-14</sup>,

and more recently for mechanical waves in phononic systems  $^{4,5,15-17}$ . The most intriguing property of these topological states is their unusual ability to guide waves around sharp structural imperfections, avoiding back-reflection from defects or disorders over broad frequency ranges  $^{4,18}$ .

In recent years, topological insulators (TI) have been developed to control phonons (elastic waves in solids) in the form of static (zero frequency floppy modes)<sup>15,19–23</sup>, and dynamical edge states<sup>5,24</sup>. Phononic systems benefit from much smaller wavelengths and stronger boson-boson interactions as compared to photonic systems operating at similar frequencies<sup>6</sup>. Specifically, mechanical TIs can be classified into two broad groups. The first actively breaks time-reversal symmetry to realize chiral edges states analogous to the quantum Hall effect (QHE)<sup>6,17</sup>, while the other one passively breaks inversion symmetry to realize helical edge states analogous to the quantum spin Hall effect  $(QSHE)^{4,18}$ . However, only breaking time-reversal symmetry guarantees complete immunity to back-scattering, regardless of the nature of the  $defect^{25}$ . In mechanical systems, breaking time reversal symmetry has been accomplished via Lorentz forces<sup>26</sup>, gyroscopes<sup>27</sup>, rotating frames<sup>6,28</sup>, and Coriolis  $forces^{17,29,30}$ . Nonetheless, experimental realizations of these complex methods are challenging and further complicated by loss and noise mechanisms associated with moving media. One possible scenario for overcoming these issues is to instead employ time-varying properties to synthesize a momentum bias<sup>31,32</sup>. Recently, Fleury et al. proposed a nonreciprocal acoustic metamaterial analogue of a Floquet topological insulator (FTI), where the material properties are modulated in time and space in a time-harmonic rotating manner<sup>25</sup>. proposed modulation scheme synthesizes an on-site rotation, without the requirement of phase uniformity across the lattice, imparting a gauge bias to the lattice that breaks time-reversal symmetry and induces topological order. This unique feature, exploited in the case of the single unit cell element to realize circulators<sup>33</sup>, can be a stepping-stone platform towards practical implementations of ultra-broadband topological

<sup>\*</sup> michael.leamy@gatech.edu

<sup>†</sup> aalu@gc.cuny.edu

insulators and acoustic diodes for mechanical waves.

While FTIs were originally introduced in quantum and photonic systems  $^{34-37}$ , experimental demonstrations time-reversal non-symmetric FTIs based time modulation have never been demonstrated experimentally to the best of our knowledge. photonics, the required time modulation would make it impractical to use electro-optical modulation. Phononic systems, while they can somewhat relax the requirements on modulation speeds, require large actuations to significantly alter the material properties in time. In this Letter we report the first design and fabrication of a phononic FTI exhibiting protected edge states. We employ piezoelectric patches connected to a negative capacitance circuit and a programmable switch to dramatically change in time and locally the effective elasticity modulus of the coupled system.

Topologically protected wave propagation from the source to the receiver (at an arbitrary location) in the proposed structure can be then controlled by a programmable switch, which implements a fully reconfigurable device in which topological order can be imparted on demand. This dynamic reconfigurability is essential to enable TI-based applications, such as signal multiplexing and de-multiplexing where the edge state pathway can be reconfigured and routed in real time.

The realized system consists of a graphene-like lattice (hexagonal honeycomb) formed by a periodic array of shunted piezoelectric disks bonded to a thin Polyactic Acid (PLA) plate. These hexagonal lattices support Dirac points, whose inherent time-reversal symmetry can be broken by the synthetic angular momentum imparted in each unit cell by the rotating spatio-temporal modulation of the lattice Young's modulus. In turn, this creates a bandgap supporting topologically protected edge states. The time modulation is implemented by external circuits with a time-modulated negative capacitance connected to the PZT disks.

### RESULTS:

## A. Topological crystal with broken time-reversal symmetry

Fig. 1(a) shows a schematic of the proposed phononic metamaterial, composed of hexagonal unit cells (shown in Fig. 1(b)) formed by 0.5 mm thick circular piezoelectric disks of diameter  $d_1 = 7$  mm and capacitance  $C_p = 1.5$  nF, attached to an elastic PLA plate of thickness  $h_0 = 0.5$  mm. Each piezoelectric disk can be viewed as an elastic resonator bonded to the top surface of the host material. Fig. 1(d) depicts the band structure for the un-modulated unit cell (red dashed lines), documenting a two-fold degeneracy at the edge of the unit cell (i.e., K-point), where two distinct Lamb modes<sup>38</sup> meet at  $f \approx 84.5$  kHz. Supplementary Note 1 provides a full discussion on the generation of these dispersion curves and their associated mode shapes.

The next step in realizing an analogue of quantum

Hall effect in this system requires breaking time-reversal symmetry and opening a topological bandgap at the Dirac point. This is achieved by connecting negative capacitance circuits to each PZT disk, while modulating these circuits by a periodic on-site potential  $\Delta C$  =  $-\delta C \times \tilde{G}(\phi)$  with strength  $\delta C$  and frequency  $f_0 = \omega_0/2\pi$ , where  $\tilde{G}(\phi) = \operatorname{sgn}\left(\cos(\omega_0 t + \phi)\right) - 1$  is the modulation function. The phase  $\phi$  in  $\tilde{G}$  depends on the considered PZT in a way such that the modulation imparts an effective spin onto each trimer. The negative capacitance obtained by the circuit depicted in Fig. 1(d) results in significant changes in the effective Young's modulus of the connected PZT disk<sup>39-41</sup>. The circuit is composed of two resistors  $(R_1 = 10, R_2 = 20 \Omega)$ , one capacitor  $(C_0 = 1nF)$ , and an operational amplifier, providing a negative capacitance of  $C' = -(R_2C_0)/R_1 = -2 nF$  (for the optimal case) when connected to the PZT in series. Finally, periodic on-off operation of the switch connecting the circuit to the PZT disk induces an effective modulus variation between  $E_m = 55 \ GPa$  (for the optimal case) and  $E_0 = 80$  GPa, with a period of  $T_0 = 2\pi/\omega_0$ . Supplementary Note 2 provides full details on calculating the modulated modulus of elasticity.

Figure 1(d) plots the band structure of the described unit cell undergoing time modulation (blue curves,  $\delta C =$ 2.5 nF and  $f_0 = 50 \ kHz$ , which documents lifting of the degeneracy at both the  $\Gamma$  and K points. It should be noted that, by further increasing the modulation strength (with  $f_0$  being unchanged), the bandgap opens until we reach a maximum bandgap with flat bands, analogous to the quantum Hall effect. Figure 1(e) displays the band structure corresponding to this optimal case for  $\delta C =$ 2nF. Further increases in the modulation strength is detrimental to gap opening width, due to pinching of the bands at the G point. It should be noted that the band structures in Fig. 1(e)-(f) are plotted for the frequency range of interest  $(79-86 \ kHz)$ ; hence, folded bands along the frequency axis are not visible. Supplementary Note 1 provides the complete band structure including all folded bands. Finally, in order to characterize the topological character of each of these four bands (plotted in blue), the corresponding Chern numbers are computed and reported as  $\{2,0,0,-2\}$  for right-handed modulation. Supplementary Note 2 also provides a full discussion of the Chern number calculations.

#### B. Emergence of topologically protected edge waves

A unique property of non-reciprocal TIs is the presence of one-way edge modes at the interface between domains with opposite topological invariants. According to the bulk-edge correspondence principle, the number of edge states at a given interface is the sum of Chern numbers of all the bulk modes below the bandgap<sup>42</sup>. In order to realize the edge states of the system, a finite  $1 \times 7$  super cell is considered. Figure 2(a) illustrates the

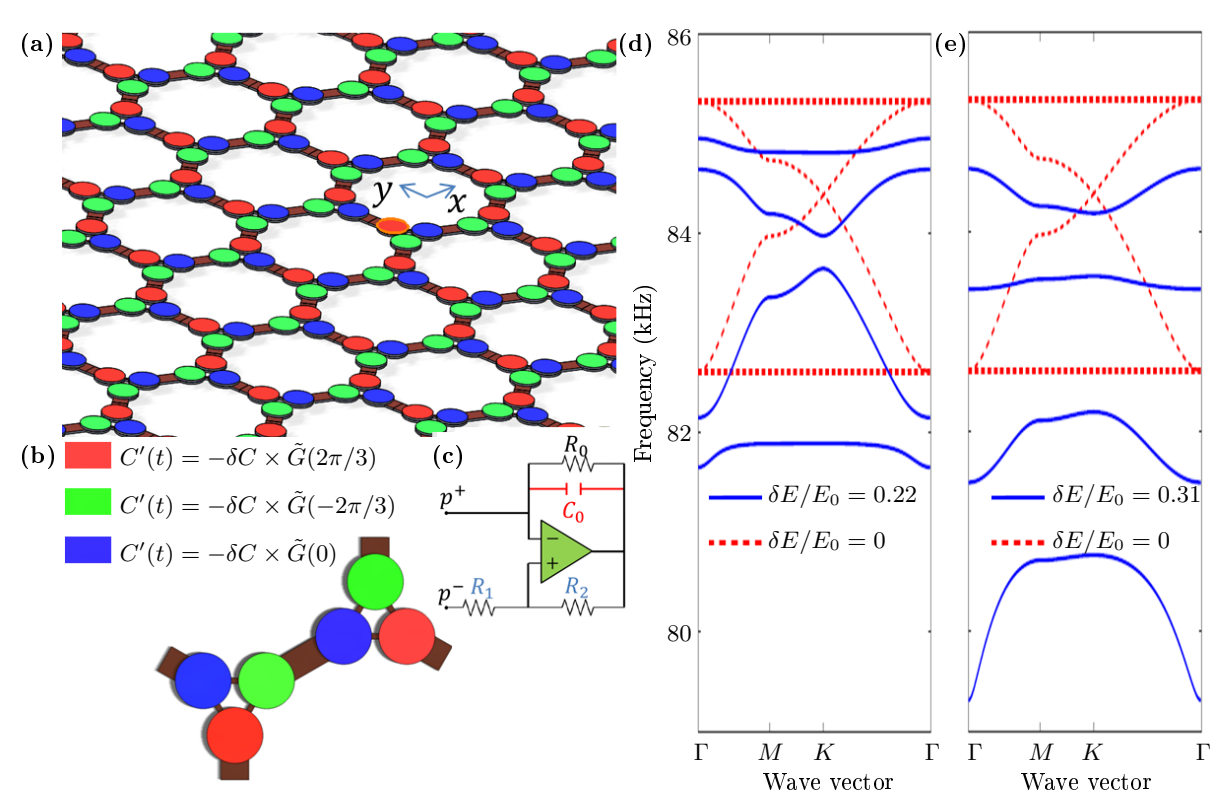


Figure 1. Time reversal symmetry breaking in a phononic crystal. (a) Schematic of the time-dependent phononic crystal formed by hexagonal unit cells with PLA ( $h_0=0.5\ mm$  thick) as the host layer and attached circular piezoelectric (PZT) patches with thickness of  $h_1=0.5\ mm$  ( $d_1=7\ mm$  in diameter). (b) The elastic modulus of each PZT patch is periodically modulated in time in a rotating manner (with uniform handedness throughout the lattice) through connections to external circuits. (c) The shunted circuits, composed of two resistors ( $R_1$ , and  $R_2$  in blue), one capacitor ( $C_0$  in red), and an op-amp, provide a negative capacitance  $C'=-(R_2C_0)/R1$ , which is altered in time by a switch that turns ON/OFF at the frequency  $f_0=\omega_0/2\pi$  with the function  $\tilde{G}(\phi)=\text{sgn}\left(\cos(\omega_0t)+\phi\right)-1$ . The resistor ( $R_0$ ) parallel to the capacitor prevents saturation of the capacitor. (d) Comparison between the band structures along the irreducible Brillouin zone perimeters in the absence (red dashed-curves with a Dirac point at  $\approx 84.5\ kHz$ ), and in the presence (blue solid-curves with modulation at  $f_0=50\ kHz$ ,  $\delta C=2.5\ nF$ ,  $\delta E/E_0=0.22$ ) of modulation. (e) Comparison between the band structures along the irreducible Brillouin zone perimeters in the absence (red dashed-curves with a Dirac point at  $\approx 84.5\ kHz$ ), and in the presence (blue solid-curves with optimal modulation at  $f_0=50\ kHz$ ,  $\delta C=2\ nF$ ,  $\delta E/E_0=0.31$ ) of modulation. The time modulation has the effect of folding the band structure along the frequency axis and lifting the degeneracy at the K and  $\Gamma$  points, opening a complete bandgap with topological protection. Supplementary Note 1 provides the complete band structure of the proposed system, showing folded frequencies in the vertical direction.

band diagram for this strip with uniform modulation handedness (see Fig. 2(b)), periodically repeated in the x-direction with the modulation strength and frequency of  $\delta C = 2~nF$  and  $f_0 = 50~kHz$ , respectively. The figure clearly reveals the existence of two distinct modes within each bandgap. Since these topologically protected edge modes are in the bandgap, they cannot scatter into the bulk of the structure and propagate only along the edges in one direction. Figure 2(b) shows the displacement field of the strip at 83 kHz (marked with a green star), documenting an edge mode localized at the top boundary.

### C. Experimental observation of topological edge modes

A set of experiments validate the performance of the proposed FTI. Fig. 3(a) depicts the experimental setup formed by bonding 150 piezoelectric disks to a 3D-printed PLA host material. Each piezoelectric disk connects to an external circuit with a programmable controller to provide space and time stiffness modulation (see Supplementary Note 3 for full details on the experimental setup). The experimentally measured frequency response of the system is depicted in Fig. 3(b) for the range  $86-90\ kHz$ , showing the transfer function between the input and the two points marked with pink and green stars in Fig. 3(c). We observe two clear bandgaps over which the transfer function is close to zero for the point (pink star)

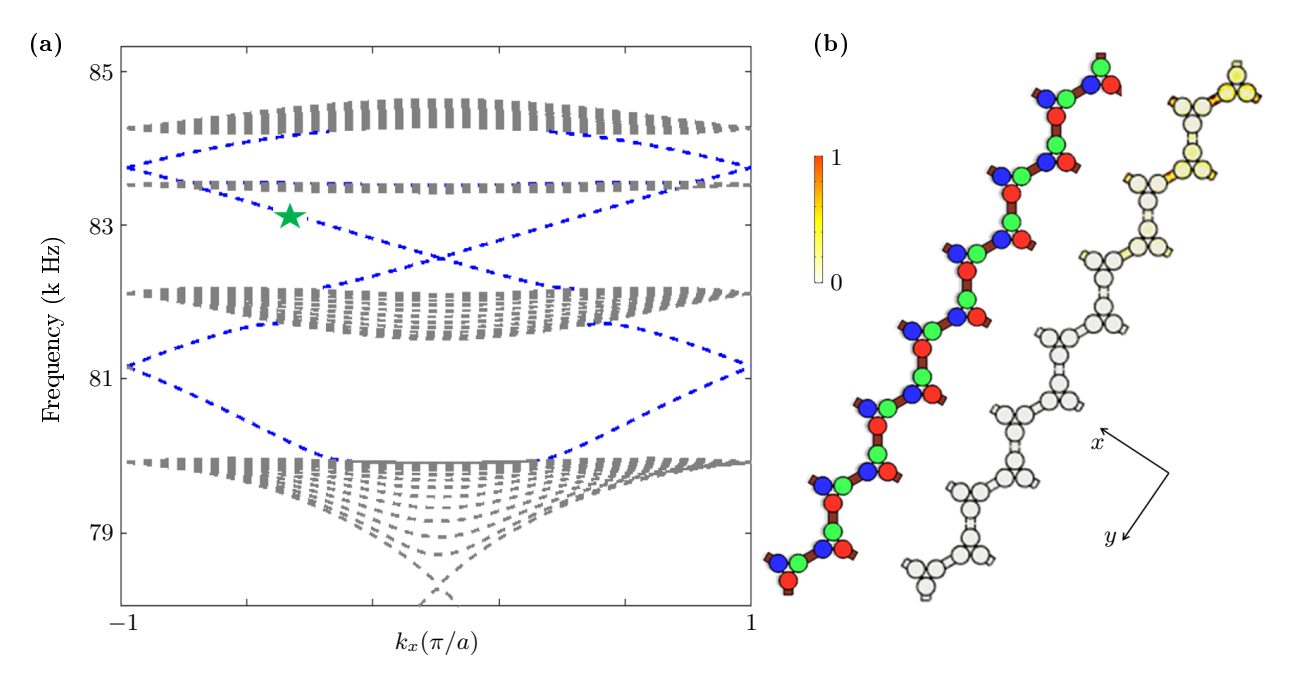


Figure 2. Numerical computation of topologically-protected edges states. (a) Quasi-band structure of a supercell composed of  $1 \times 7$  arrays of unit cells, periodically repeated in the x-direction and analyzed using Floquet boundary conditions. Gray areas depict bulk bands and blue dashed lines depict the edge modes. (b) Schematic of the super-cell and the corresponding wave distribution at frequency  $f = 83 \ kHz$  (marked with a green star), showing wave localization at the top edge. All displacements are normalized by the maximum deformation of the cell.

within the bulk, while for the point on the edge (green star) two edge modes support transmission close to unity, ensuring efficient transport for the fabricated structure. Figure 3(c) exhibits the experimentally measured RMS wavefield resulting from excitation at  $89.5\ kHz$ . Due to the imperfections in the experimental setup, and stiffness of connected wires, this frequency is slightly above the one predicted using numerical modeling. The provided figure clearly confirms the presence of QHE-like edge modes at the free interface.

To study wave propagation at the interface of two domains with opposite Chern numbers, and show realtime reconfigurability, we change the topological features of our sample by modifying the modulation pattern. 4a. we divide the sample in two regions: one subdomain experiences a right-handed synthetic angular momentum modulation, and the other subdomain a left-handed one; therefore, they share a topologically protected domain wall where localized waves can propagate one-way and without scattering into the bulk. Figure 4(a) reports the RMS response of the system at  $89.5 \ kHz$  for a horizontal interface, exhibiting wave propagation from a source on the right side to a receiver on the left side of the structure. As another example, Fig. 4(d) shows the response of the system at the same frequency for a different modulation scheme, forming a triangular domain wall. As shown, waves travel from the source on the right side to reach the receiver at the top of the structure, with minimal scattering at the sharp edge. In order to clearly observe propagation of

the wave at the interfaces, return wave propagation at the edges is prevented in this case by sticking absorbing pitches on the perimeter. Supplementary Note 3 shows snapshots in time of the propagating modes during the transient excitation for the experiments in Figure 4 at various instances of time from the start of the excitation, showing the time evolution from the transient response to steady-state.

### DISCUSSION

In summary, this Letter reports the first experimental implementation of a non-reciprocal Floquet topological insulator based on synthetic angular momentum bias. implemented using spatio-temporal modulation in elastodynamics. A unit cell composed of a PLA host layer bonded to six time-modulated piezoelectric disks is biased by a synthetic angular momentum imparted by a rotating phase of the modulation signal, which breaks time-reversal symmetry. The time modulation of the PZT disks is implemented using external circuits with effective negative capacitance. Numerical simulations document a topologically-protected bandgap with edge states connecting the bulk modes. Experimental measurements nicely confirm these predictions by demonstrating topologically-protected, back-scattering immune wave propagation along edges and interfaces. The modulation network is directly amenable to provide reconfigurability: by simply controlling the capacitance

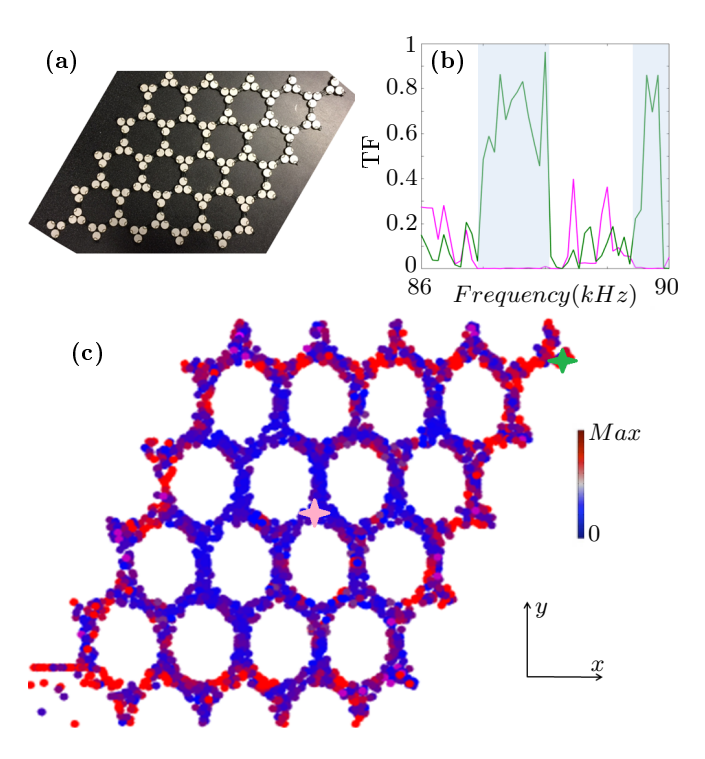


Figure 3. Experimentally-measured edge states. (a) Fabricated topological insulator configured to exhibit an edge mode on free surfaces for a uniform right-handed synthetic angular momentum imparted by the spatiotemporal modulation. Each PZT is connected to an external circuit. (b) Experimentally measured transfer function at the two points marked with pink and green stars. The light blue areas show the topological bandgap. (c) Experimentally-measured RMS displacement field excited by a source with frequency  $89.5\ kHz$ , documenting wave propagation along the free edges without back-scattering. All displacements have been normalized to the amplitude of the input wave.

of the circuits, reconfigurable domain walls have also been experimentally demonstrated. The fabricated metamaterial represent an advantageous platform to realize acoustic multiplexers, de-multiplexers, and mechanical logic elements in engineered systems.

J. E. Moore, The birth of topological insulators, Nature 464, 194 (2010).

Y. Chen, J. G. Analytis, J.-H. Chu, Z. Liu, S.-K. Mo, X.-L. Qi, H. Zhang, D. Lu, X. Dai, Z. Fang et al., Experimental realization of a three-dimensional topological insulator, bi2te3, science 325, 178 (2009).

<sup>&</sup>lt;sup>3</sup> L. Lu, J. D. Joannopoulos, and M. Soljačić, Topological photonics, Nature Photonics 8, 821 (2014).

<sup>&</sup>lt;sup>4</sup> S. H. Mousavi, A. B. Khanikaev, and Z. Wang, Topologically protected elastic waves in phononic metamaterials, Nature communications **6**, 8682 (2015).

<sup>&</sup>lt;sup>5</sup> R. Süsstrunk and S. D. Huber, Observation of phononic helical edge states in a mechanical topological insulator, Science 349, 47 (2015).

<sup>&</sup>lt;sup>6</sup> A. B. Khanikaev, R. Fleury, S. H. Mousavi, and A. Alù, Topologically robust sound propagation in an angularmomentum-biased graphene-like resonator lattice, Nature communications 6, 8260 (2015).

<sup>&</sup>lt;sup>7</sup> M. Z. Hasan and C. L. Kane, Colloquium: topological insulators, Reviews of Modern Physics 82, 3045 (2010).

<sup>&</sup>lt;sup>8</sup> X.-L. Qi and S.-C. Zhang, Topological insulators and superconductors, Reviews of Modern Physics 83, 1057 (2011).

<sup>&</sup>lt;sup>9</sup> K. Von Klitzing, The quantized hall effect, Reviews of Modern Physics 58, 519 (1986).

<sup>&</sup>lt;sup>10</sup> C. L. Kane and E. J. Mele, Quantum spin hall effect in graphene, Physical review letters 95, 226801 (2005).

F. Haldane and S. Raghu, Possible realization of directional optical waveguides in photonic crystals with broken time-reversal symmetry, Physical review letters 100, 013904 (2008).

<sup>&</sup>lt;sup>12</sup> Z. Wang, Y. Chong, J. D. Joannopoulos, and M. Soljačić, Reflection-free one-way edge modes in a gyromagnetic photonic crystal, Physical review letters **100**, 013905 (2008).

A. B. Khanikaev, S. H. Mousavi, W.-K. Tse, M. Kargarian, A. H. MacDonald, and G. Shvets, Photonic topological insulators, Nature materials 12, 233 (2013).

<sup>&</sup>lt;sup>14</sup> M. Hafezi, S. Mittal, J. Fan, A. Migdall, and J. Taylor, Imaging topological edge states in silicon photonics,

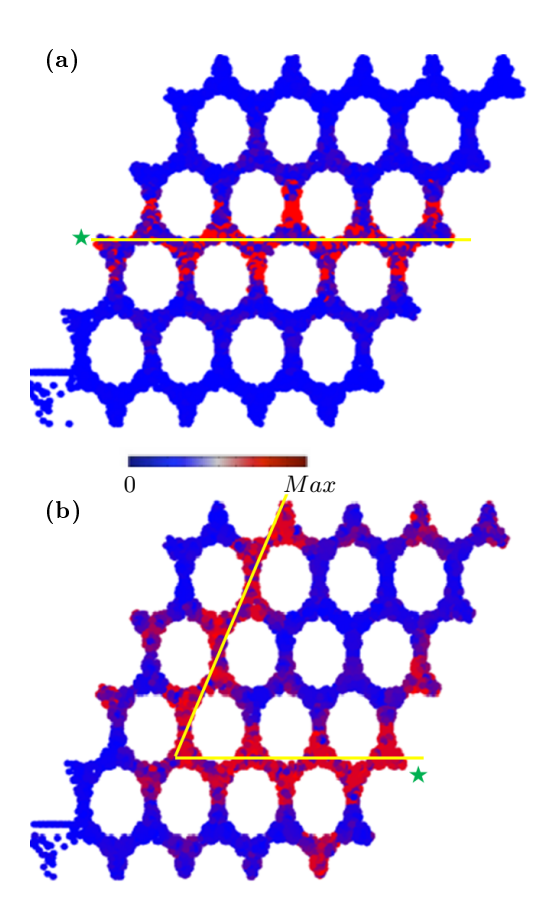


Figure 4. Experimentally-measured domain-wall states. Experimentally measured RMS displacement field of the system excited by a source (marked with a green star) with frequency  $89.5\ kHz$ , documenting immune to back-scattering wave propagation along (a) a horizontal domain wall, and (b) a triangular-shaped domain wall, created by modulating different regions of the lattice with oppositely handed synthetic angular momentum. All displacements have been normalized to the amplitude of the input wave. For these interfaces, modulation of unit cells on one side of the yellow line is right-handed, and on the other side is left-handed.

Nature Photonics 7, 1001 (2013).

<sup>15</sup> J. Paulose, B. G.-g. Chen, and V. Vitelli, Topological modes bound to dislocations in mechanical metamaterials, Nature Physics 11, 153 (2015).

<sup>16</sup> B. G.-g. Chen, N. Upadhyaya, and V. Vitelli, Nonlinear conduction via solitons in a topological mechanical insulator, Proceedings of the National Academy of Sciences 111, 13004 (2014).

<sup>17</sup> R. Fleury, D. L. Sounas, C. F. Sieck, M. R. Haberman, and A. Alù, Sound isolation and giant linear nonreciprocity in a compact acoustic circulator, Science 343, 516 (2014).

<sup>18</sup> M. Miniaci, R. Pal, B. Morvan, and M. Ruzzene, Experimental observation of topologically protected helical edge modes in patterned elastic plates, Physical Review X 8, 031074 (2018).

<sup>19</sup> C. Kane and T. Lubensky, Topological boundary modes in isostatic lattices, Nature Physics 10, 39 (2014).

D. Z. Rocklin, B. G.-g. Chen, M. Falk, V. Vitelli, and T. Lubensky, Mechanical weyl modes in topological

maxwell lattices, Physical review letters 116, 135503 (2016).

<sup>21</sup> O. Stenull, C. Kane, and T. Lubensky, Topological phonons and weyl lines in three dimensions, Physical review letters 117, 068001 (2016).

O. R. Bilal, R. Süsstrunk, C. Daraio, and S. D. Huber, Intrinsically polar elastic metamaterials, Advanced Materials 29, 1700540 (2017).

<sup>23</sup> E. Prodan, K. Dobiszewski, A. Kanwal, J. Palmieri, and C. Prodan, Dynamical majorana edge modes in a broad class of topological mechanical systems, Nature communications 8, 14587 (2017).

<sup>24</sup> T. Kariyado and Y. Hatsugai, Manipulation of dirac cones in mechanical graphene, Scientific reports **5**, 18107 (2015).

<sup>25</sup> R. Fleury, A. B. Khanikaev, and A. Alu, Floquet topological insulators for sound, Nature communications 7, 11744 (2016).

E. Prodan and C. Prodan, Topological phonon modes and their role in dynamic instability of microtubules, Physical review letters 103, 248101 (2009).

<sup>27</sup> P. Wang, L. Lu, and K. Bertoldi, Topological phononic crystals with one-way elastic edge waves, Physical review letters 115, 104302 (2015).

<sup>28</sup> L. M. Nash, D. Kleckner, A. Read, V. Vitelli, A. M. Turner, and W. T. Irvine, Topological mechanics of gyroscopic metamaterials, Proceedings of the National Academy of Sciences 112, 14495 (2015).

<sup>29</sup> Y.-T. Wang, P.-G. Luan, and S. Zhang, Coriolis force induced topological order for classical mechanical vibrations, New Journal of Physics 17, 073031 (2015).

<sup>30</sup> X. Ni, C. He, X.-C. Sun, X.-p. Liu, M.-H. Lu, L. Feng, and Y.-F. Chen, Topologically protected one-way edge mode in networks of acoustic resonators with circulating air flow, New Journal of Physics 17, 053016 (2015).

R. Chaunsali, E. Kim, A. Thakkar, P. G. Kevrekidis, and J. Yang, Demonstrating an in situ topological band transition in cylindrical granular chains, Physical review letters 119, 024301 (2017).

<sup>32</sup> N. Swinteck, S. Matsuo, K. Runge, J. Vasseur, P. Lucas, and P. A. Deymier, Bulk elastic waves with unidirectional backscattering-immune topological states in a time-dependent superlattice, Journal of Applied Physics 118, 063103 (2015).

N. A. Estep, D. L. Sounas, J. Soric, and A. Alù, Magnetic-free non-reciprocity and isolation based on parametrically modulated coupled-resonator loops, Nature Physics 10, 923 (2014).

M. C. Rechtsman, J. M. Zeuner, Y. Plotnik, Y. Lumer, D. Podolsky, F. Dreisow, S. Nolte, M. Segev, and A. Szameit, Photonic floquet topological insulators, Nature 496, 196 (2013).

<sup>35</sup> J.-i. Inoue and A. Tanaka, Photoinduced transition between conventional and topological insulators in twodimensional electronic systems, Physical review letters 105, 017401 (2010).

<sup>36</sup> N. H. Lindner, G. Refael, and V. Galitski, Floquet topological insulator in semiconductor quantum wells, Nature Physics 7, 490 (2011).

<sup>37</sup> B. Dóra, J. Cayssol, F. Simon, and R. Moessner, Optically engineering the topological properties of a spin hall insulator, Physical review letters 108, 056602 (2012).

<sup>38</sup> H. Lamb, On waves in an elastic plate, Proc. R. Soc. Lond. A **93**, 114 (1917).

- <sup>39</sup> S. Behrens, A. Fleming, and S. Moheimani, A broadband controller for shunt piezoelectric damping of structural vibration, Smart materials and structures 12, 18 (2003).
- <sup>40</sup> B. S. Beck, K. A. Cunefare, and M. Collet, The power output and efficiency of a negative capacitance shunt for vibration control of a flexural system, Smart Materials and Structures 22, 065009 (2013).
- <sup>41</sup> N. W. Hagood and A. von Flotow, Damping of structural vibrations with piezoelectric materials and passive electrical networks, Journal of Sound and Vibration 146, 243 (1991).
- <sup>42</sup> Y. Hatsugai, Chern number and edge states in the integer quantum hall effect, Physical review letters **71**, 3697

(1993).

### I. ACKNOWLEDGMENTS

The authors would like to thank the National Science Foundation for supporting this research under Grant No. 1929849. AA acknowledges support from the National Science Foundation.

### II. COMPETING FINANCIAL INTERESTS

The authors declare no competing financial interests.